Chemical Engineering Journal 346 (2018) 567–577

Contents lists available at ScienceDirect

Chemical Engineering Journal

journal homepage: www.elsevier.com/locate/cej

Heterogeneous photo-Fenton degradation of bisphenol A over Ag/AgCl/ferrihydrite catalysts under visible light

Yanping Zhu[a,b], Runliang Zhu[a,*], Yunfei Xi[c], Tianyuan Xu[a,b], Lixia Yan[a,b], Jianxi Zhu[a], Gangqiang Zhu[d,*], Hongping He[a]

[a] CAS Key Laboratory of Mineralogy and Metallogeny/Guangdong Provincial Key Laboratory of Mineral Physics and Materials Research & Development, Guangzhou Institute of Geochemistry, Chinese Academy of Sciences(CAS), Guangzhou 510640, China
[b] University of Chinese Academy of Sciences, Beijing 100049, China
[c] Institute for Future Environments, Queensland University of Technology (QUT), Brisbane, Queensland 4001, Australia
[d] School of Physics and Information Technology, Shaanxi Normal University, Xi'an 710062, China

HIGHLIGHTS

- Novel Ag/AgCl/Fh photo-Fenton catalysts were synthesized.
- Plasmonic Ag/AgCl particles can significantly accelerate the redox cycling of Fe^{2+}/Fe^{3+}.
- The degradation rate constant of BPA over 6%Ag/AgCl/Fh is nearly about 5.1 times as high as that of pure Fh.
- Ag/AgCl/Fh exhibit very high photo-Fenton catalytic activity even at pH 6.
- Mechanisms for enhanced photo-Fenton catalytic activity of Ag/AgCl/Fh were investigated.

GRAPHICAL ABSTRACT

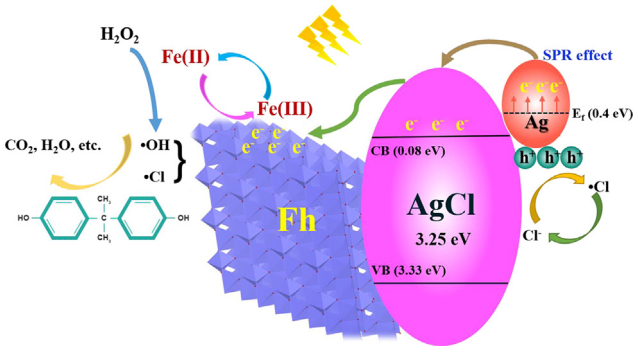

ARTICLE INFO

Keywords:
Ag/AgCl
Ferrihydrite
Photo-Fenton
Surface plasmon resonance
Photo-generated electrons

ABSTRACT

The conventional heterogeneous Fenton reaction is often confined by the lower regeneration of Fe^{2+}, which then inhibits the decomposition of H_2O_2 and the generation of ·OH. Here we propose a novel idea to significantly accelerate the redox cycling of Fe^{2+}/Fe^{3+} in heterogeneous Fenton reaction by introducing photo-generated electrons from plasmonic particles. Towards this aim, novel plasmonic Ag/AgCl nanoparticles coated ferrihydrite (Ag/AgCl/Fh) have been synthesized. Compared with pure Fh, a remarkable enhancement in the photo-Fenton degradation towards bisphenol (BPA) can be observed for all Ag/AgCl/Fh samples under visible light. Noticeably, the rate constant of 6%Ag/AgCl/Fh is 0.0506 min^{-1}, which is about 5.1 times as high as that of pure Fh (0.0099 min^{-1}). Moreover, the catalytic activity of 6%Ag/AgCl/Fh on the degradation of BPA remains quite efficient with a low Fe leaching after 4 recycles. The results of the effect of initial pH indicates that Ag/AgCl/Fh samples exhibit relatively high photo-Fenton catalytic activity even at pH 6. The electron spin resonance (ESR) analysis reveals that ·OH plays a significant role in the photo-Fenton reaction. The concentration of ·OH can even reach 267.6 μmol/L after 60 min, which is much higher than that of pure Fh (69.2 μmol/L). The measurement of Fe^{2+} concentration and the XPS Fe2p spectra of Ag/AgCl/Fh before and after the degradation of BPA indicate the loading of Ag/AgCl can accelerate the conversion of Fe^{3+}/Fe^{2+} by the photo generated

* Corresponding authors.
E-mail address: zhurl@gig.ac.cn (R. Zhu).

https://doi.org/10.1016/j.cej.2018.04.073
Received 9 January 2018; Received in revised form 12 April 2018; Accepted 12 April 2018
Available online 13 April 2018
1385-8947/

electrons from Ag nanoparticles due to the surface plasmon resonance (SPR) effect under the visible light irradiation.

1. Introduction

In recent years, homogeneous Fenton reactions have been applied in the field of environmental remediation due to a large amount of hydroxyl free radical (·OH) generated in the reactions [1–8]. The oxidation ability of ·OH (φ^o = 2.73 V) is much stronger than most other active species, such as H_2O_2 (φ^o = 1.78 V) and ozone (φ^o = 2.08 V), which makes ·OH powerful to degrade most organic contaminants to the mineral end products in a non-selective way [9,10]. Conventional homogeneous Fenton process occurs in an acidic Fe^{2+}/H_2O_2 aqueous system [2,11–13]. However, its applications are limited mainly due to the following drawbacks: (i) low regeneration rate of Fe^{2+}, (ii) tight range of optimum pH (2.5–3.5), and (iii) excessive amounts of generated ferric hydroxide sludge [14,15].

In order to solve above problems, heterogeneous Fenton-like reactions have been developed which show great potential to replace the conventional homogeneous Fenton reactions [10,16,17]. Recently, a great deal of attention has been paid to the heterogeneous Fenton-like catalysts such as Fe_3O_4 [10,18], α-Fe_2O_3 (Liu et al., 2017), γ-Fe_2O_3 [19], α-FeOOH [20], β-FeOOH [21], and $ZnFe_2O_4$ [22]. Among them, ferrihydrite (Fh) nanoparticles have attracted much research interests recently as it is a naturally occurring Fe (III) hydroxide nanomineral with a large specific surface area (SSA > 200 m^2/g) [23–26]. Nevertheless, the catalytic efficiency of the Fh nanoparticles awaits further improvement due to the relatively low regeneration rate of Fe^{2+} (by reducing Fe^{3+} to Fe^{2+}) during the Fenton reaction.

For the purpose of improving the regeneration rate of Fe^{2+}, recently many studies have focused on introducing semiconductors to the photo-Fenton system, such as $BiVO_4$@Fh [23], Fe_3O_4@rGO@TiO_2 [10], SiO_2/Fe_3O_4/C@TiO_2 [9], and $BiOIO_3/Fe_2O_3$ [27]. The photogenerated electrons from these semiconductors accelerate the conversion of Fe^{3+}/Fe^{2+}, which then promote the decomposition of H_2O_2 into ·OH. These studies enlighten us that introducing in-situ generated electrons to the heterogeneous Fenton catalysts might be an effective strategy for enhancing their photo-Fenton reactivity.

In recent years, the Ag/AgX (Cl, Br, I) catalysts have become the focus of research in the field of photocatalysis because of the surface plasmon resonance (SPR) effect under visible light [28–39]. These photocatalysts can nearly absorb entire visible light and generate electrons and holes through the collective oscillations of the surface electrons [40]. However, pure Ag/AgCl composites usually aggregate to micrometer-scale particles size, resulting in low surface areas and high recombination rate of the photo generated charge carriers [41]. In this regard, we propose that combining Ag/AgCl with Fh may achieve exciting novel composites with high photo-Fenton reactivity, as the generated electrons from Ag/AgCl can help in reducing Fe^{3+} on Fh, and Fh may have a tailoring effect on Ag/AgCl to inhibit its aggregation (because of the large surface areas and plenty of reactive surface sites of Fh).

In this study, we have synthesized Ag/AgCl/Fh heterogeneous photocatalysts via a multistep route by loading the different content of Ag/AgCl on the surface of Fh. The structural and photoelectrochemical characteristics of Ag/AgCl/Fh samples have been studied. The obtained Ag/AgCl/Fh catalysts exhibited remarkably enhanced photo-Fenton catalytic activity for the degradation of BPA under visible light. It may result from the SPR effect of Ag nanoparticles and the fast carrier transfer between the active materials in the composites.

2. Experiment

2.1. Materials

Fe $(NO_3)_3·9H_2O$ (AR), $AgNO_3$ (AR), NaCl (AR), NaOH (AR), HCl (AR), and hydrogen peroxide (30 wt%) were obtained from Shanghai Chemical Reagent Corporation, China. Bisphenol A was purchased from Macklin Reagent Company. Benzoic acid (99.5%) and p-hydroxybenzoic acid (99%) were obtained from Aladdin Industrial Corporation (Shanghai, China). All labware were cleaned by soaking overnight in dilute HCl solution and washed in ultra-pure water (> 18 MΩ/cm) before experiments.

2.2. Synthesis of Fh

Two-line Fh was synthesized as follows: 50 mL Fe $(NO_3)_3·9H_2O$ (1 mol/L) and 30 mL NaOH (4 mol/L) were simultaneously dropped into a beaker with vigorous stirring, and the final pH was adjusted to 7.0 [42]. After stirring for 2 h, the mixture was centrifuged and washed with ultra-pure water and alcohol for 5 times. After being freeze-dried, the material was ground to sieve through a 200-mesh sieve.

2.3. Synthesis of Ag/AgCl/Fh

According to Gamage McEvoy et al. [43], and with a slight modification, Ag/AgCl/Fh were prepared via an impregnation-precipitation-photo reduction method. As shown in Scheme 1, an appropriate amount of $AgNO_3$ (0.016, 0.047, 0.094, and 0.157 g) and Fh powder (1 g) were added to 20 mL ultra-pure water. The mixture was sonicated for 30 min and then stirred for 30 min to disperse the Ag^+ on the surface of Fh thoroughly. After that, 20 mL excess NaCl solution (9.26–92.6 mM) was dropped slowly into the mixture solution, which can induce the precipitation of deposited $AgNO_3$ into AgCl completely. After stirring for 30 min, 10 mL methanol (as a hole scavenger) was

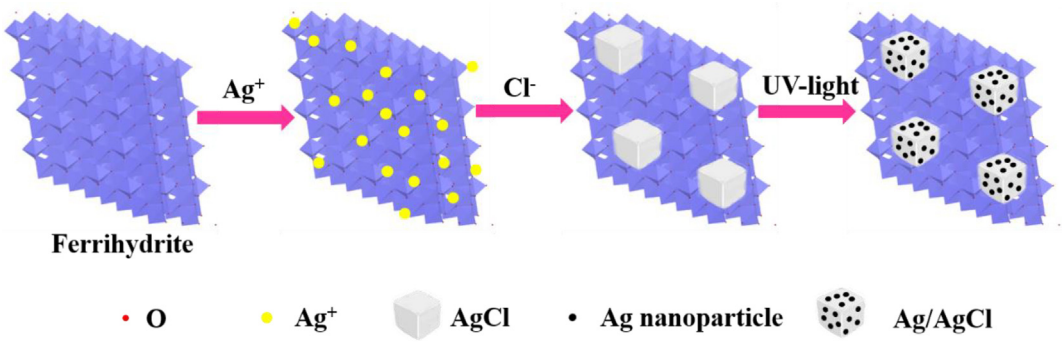

Scheme 1. Schematic illustration for the preparation of Ag/AgCl/Fh.

added to the above solution. Subsequently, the resulting suspension was placed under irradiation of a 300 W mercury lamp (BL-GHX-V, Shanghai Depai Biotech. Co. Ltd., China) for 1 h. The obtained precipitates were washed with ultra-pure water and alcohol for 5 times, and then freeze-dried. According to the weight ratio of added Ag to Fh, the samples are labeled as 1%Ag/AgCl/Fh, 3%Ag/AgCl/Fh, 6%Ag/AgCl/Fh, and 10%Ag/AgCl/Fh, respectively.

2.4. Characterization

XRD patterns were obtained using a Bruker D8 ADVANCE X-ray diffractometer (Karlsruhe, Germany) equipped with Cu K-alpha radiation (40 kV, 40 mA). The scanning electron microscopy (SEM) images were recorded by a field emission scanning electron microscopy (Carl Zeiss SUPRA55SAPPHIR). Transmission electron microscopy (TEM) images were acquired using FEI Talos F200S instrument at an acceleration voltage of 200 kV with energy dispersive X-ray spectroscopy (EDS) for the determination of metal composition. The UV–vis diffuse reflectance spectra (DRS) were recorded on a UV–vis spectrometer (Shimadzu UV-2550) using $BaSO_4$ as an absorbance standard. X-ray photoelectron spectroscopy (XPS) analyses were carried out by a Thermo Fisher Scientific K-Alpha spectrometer. All the binding energies were referenced to C1s peak at 284.80 eV of the surface adventitious carbon. The AgCl photoanode and Pt sheet were used as the working electrode and counter electrode respectively. X-band ESR spectra were recorded by a Bruker EMX-10/12 microspectrometer at 90 K. The operating frequency and power are 9.43 GHz and 19.83 mW, respectively. All the measurements were carried out in the presence of 300 W xenon lamp. Samples were placed into NMR tubes and cooled to 90 K by the use of liquid nitrogen stream for measurements.

2.5. Photo-Fenton catalytic experiments

The degradation of BPA by the obtained materials was monitored in a photochemical reaction instrument (PCX50A Discover, Beijing Perfectlight Technology Co., Ltd, Beijing, China). A 5 W LED lamp (148.5 mW/cm^2) was used as a cold light source. Details of the LED Lamps and photographs of the photo-Fenton experimental setup were provided (Figs. S1 and S2, and Table S1). The initial pH (pH = 3) was adjusted by 0.2 mol/L HNO_3 and NaOH. Before irradiation, a mixture of 50 mL BPA (30 mg/L) solution and 50 mg catalyst was vigorously stirred in the dark for 30 min to reach the adsorption–desorption equilibrium between the samples and BPA. At a given time interval, the suspension was collected, and filtered with 0.22 μm membrane filters. The experiments were conducted in duplicate and the error bars were added in the figures.

The concentration of the filtrates was quantitatively analyzed using an HPLC (Agilent 1260) equipped with a Luna 5μ C18 column (150 mm) and a UV absorbance detector. The mobile phase is acetonitrile and water (40:60, v/v) with a flow rate of 0.5 mL/min and an injection volume of 50 μL. The analysis wavelength was selected as 276 nm, which was determined using the UV–vis absorption spectrum of BPA (Fig. S3). The total organic carbon (TOC) was measured by using a Shimadzu TOC-V total organic carbon analyzer. The total Fe ions leaching was determined by atomic absorption spectrophotometry (AAS, PerkinElmer AAnalyst 400, America). The concentration of H_2O_2 was calculated by adding 3 mL of $K_2TiO(C_2O_4)_2$ (10 mM in 2.4 M H_2SO_4), which formed an orange complex (pertitanic acid) with maximum absorption at 400 nm. The concentration of pertitanic acid was measured via UV–vis spectroscopy [23,44].

The concentration of Fe^{2+} on the surface of as-prepared samples was measured according to the method of Xu et al. 2017 [23] with some modifications, which was according to a common method for the measurement of Fe(II) in the iron ore. At a given time interval, the suspension in the photo-Fenton reaction was centrifuged and the supernatant liquid was removed immediately. After that, 1 mL 6 M hydrochloric acid was added to dissolve the catalysts totally. At the same time, 0.2 g Na_2CO_3 was added to produce inert gases (e.g., CO_2) to protect Fe^{2+} being oxidized to Fe^{3+}. Then 2 mL 10 M NH_4F was dropped to remove the interference of Fe^{3+}. After that, the concentration of Fe^{2+} was measured via UV–vis spectroscopy by adding 1 mL $CH_3COONH_4-CH_3COOH$ buffer solution (pH 4.2) and 1 mL 0.5% (m/v) o-phenanthroline with a maximum absorption at 510 nm.

To quantify the production of ·OH in the process of Fenton-photo catalysis, a probe reaction was conducted by oxidizing benzoic acid (BA) to p-hydroxybenzoic acid (p-HBA) [45,46]. Joo et al. [45] found that only 10 mM BA can capture more than 99% ·OH even in the presence of 5 mM Fe^{2+} with negligible oxidation of p-HBA. Therefore, the concentration of BA was chosen as 10 Mm, and the initial pH value of the solution was 3. The *p*-HBA was also quantitatively analyzed using the Agilent 1260 HPLC equipped with a Luna 5μ C18 column (250 mm). The mobile phase was a mixture of acetonitrile and 0.1% trifluoroacetic acid aqueous solution (35:65, v/v) at a flow rate of 1 mL/min, with the detection wavelength at 255 nm [45,47]. The detection limit of p-HBA is 0.1 μM.

3. Results and discussion

3.1. Structural characterization

The XRD patterns of Ag/AgCl, Fh, and Ag/AgCl/Fh were investigated (Fig. 1). AgCl shows four distinct reflections at 27.8°, 32.2°, 46.2°, and 54.8°, which can be ascribed to the (1 1 1), (2 0 0), (2 2 0), and (3 1 1) diffraction planes, respectively, well consistent with the crystalline phase of cubic AgCl (JCPDS 31-1238). The reflection at 38.1° (1 1 1) can be assigned to the reduced Ag nanoparticles (JCPDS 04-0783). The patterns of all Ag/AgCl/Fh samples show two broad reflections at 35° and 63°, consistent with that in a previous report for 2-line Fh [42], indicating that the incorporation of Ag/AgCl doesn't have

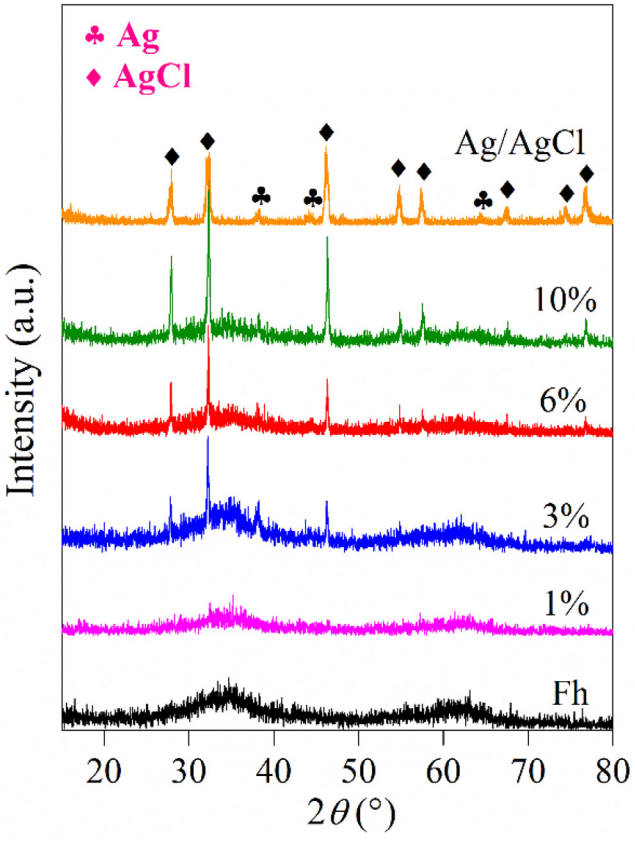

Fig. 1. XRD patterns of Ag/AgCl/Fh with various Ag contents.

a noticeable effect on the crystal structure of Fh.

The morphologies of Ag/AgCl, Fh, and 6%Ag/AgCl/Fh were examined by SEM (Fig. 2). Fh presents the aggregation of nanoparticles. The SEM image of Ag/AgCl shows that Ag nanoparticles with diameters in the range of 5–50 nm are deposited on the surface of agglomerate AgCl. As for 6%Ag/AgCl/Fh, AgCl uniformly disperses on the surface of Fh without aggregation and presents a cube-like morphology with a size of about 500 nm. Some tiny nanoparticles, which can be attributed to the Ag nanoparticles, are distributed on the surface of the Ag/AgCl.

The microstructural and morphological details of 6%Ag/AgCl/Fh were further observed by TEM and HRTEM (Fig. 3). The lattice fringes show the interplanar spacing of 0.201 and 0.234 nm, which are corresponded to the (2 0 0) and (0 0 6) lattice plane of Ag nanoparticles, while 0.278 nm is indexed to the (2 0 0) plane of AgCl. These results further confirm the existence of Ag nanoparticles on the surface of AgCl. The EDS mapping shows that the Fe, O, Ag and Cl elements of 6%Ag/AgCl/Fh are well distributed in the region.

The DRS spectra of Fh, Ag/AgCl, and Ag/AgCl/Fh were also collected (Fig. 4). The DRS spectrum of Ag/AgCl presents a broad band at 400–600 nm, which might be resulted from the SPR effect of Ag nanoparticles [48,49]. Pure Fh exhibits absorption over the whole visible region. After loading Ag/AgCl on the surface of Fh, the DRS spectral intensity of Ag/AgCl/Fh increased with increasing Ag/AgCl content.

The XPS measurements were carried out to elucidate the chemical state of the elements on the surface of the 6%Ag/AgCl/Fh (Fig. 5). The narrow region spectra for Fe $2p_{3/2}$ (Fig. 5a) are composed of three peaks at 710.2, 711.3 and 713.4 eV, which are attributed to the binding energies of Fe(III)–O in Fh [25,50]. The O 1s spectrum (Fig. 5b) is fitted with two peaks located at 529.6 and 531.2 eV, which correspond to the "O" atoms in oxide and hydroxyl, respectively [51]. The Ag 3d region (Fig. 5c) has two distinct peaks, which can be further divided into four peaks at 367.1, 368.0, 373.1, and 374.0 eV, respectively. The peaks at 367.7 and 373.7 eV are attributed to Ag^+, while those at 368.1 and 374.1 eV correspond to metallic Ag^0 [52,53]. Besides, the spectrum of Cl 2p (Fig. 5d) can be fitted with two peaks at 197.2 and 198.9 eV, which can be assigned to Cl $2p_{3/2}$ and Cl $2p_{1/2}$ in AgCl, respectively [54]. The XPS analysis further confirms the presence of Ag^0 in the 6%Ag/AgCl/Fh composites.

3.2. Photo-Fenton degradation of BPA

To validate the photo-Fenton catalytic activity of Ag/AgCl/Fh samples, several photo-Fenton catalytic experiments were examined by the degradation of BPA (Fig. 6). Except for the blank, all of the experiments were conducted by adding 10 mM H_2O_2. According to the results, lower than 10% BPA can be removed in the dark (Fig. 6a), indicating relatively poor adsorption efficiency of BPA on the as-prepared catalysts. After being irradiated, negligible degradation efficiency is obtained by visible light alone. The degradation rate of BPA for pure H_2O_2 in the dark is about 7.0%, which has no obvious changes after the irradiation of visible light (Fig. S4). The reason may be that H_2O_2 can weakly absorb visible light (Fig. S5) and the main contribution of the degradation of BPA is the weak oxidation capacity of H_2O_2 [55]. As for Fh, about 54.0% degradation and 39.5% TOC removal rates of BPA (Fig. 6b) are reached. After loading with Ag/AgCl, the degradation efficiency of BPA first increases with increasing the content of Ag/AgCl, and then it begins to decrease as the content of Ag/AgCl exceeds 6%. More specifically, 95% BPA can be degraded in 30 min by 6%Ag/AgCl/Fh, but only 32.7% BPA is degraded by pure Fh. After 60 min, the degradation rate of BPA can even reach 100% (92.0% for TOC removal rate) by 6% Ag/AgCl/Fh.

The degradation kinetics of BPA were fitted with the pseudo-first-order equation (with the obtained linearly dependent coefficients all over 0.97). The apparent rate constants are determined from the regression curves of $-\ln(C/C_0)$ versus irradiation time (Fig. 6c), in which the value of the rate constant (K_{app}) is equal to the corresponding slope of the fitting line. The K_{app} of 6%Ag/AgCl/Fh is 0.0506 min^{-1}, about 5.1 times as high as that of pristine Fh (0.0093 min^{-1}). This result proves that modification of Fh with an appropriate amount of Ag/AgCl can significantly increase the photo-Fenton catalytic activity towards BPA.

To test the stability of the catalysts, Fe ions leaching during the

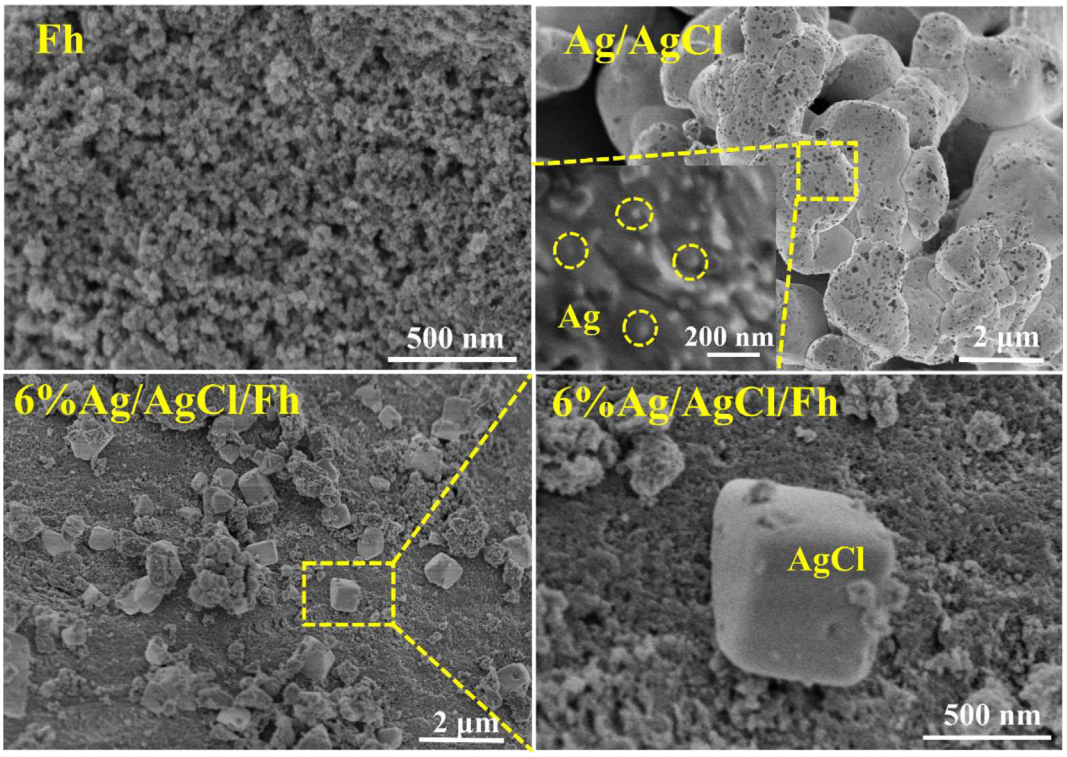

Fig. 2. SEM images of Fh, Ag/AgCl, and 6%Ag/AgCl/Fh.

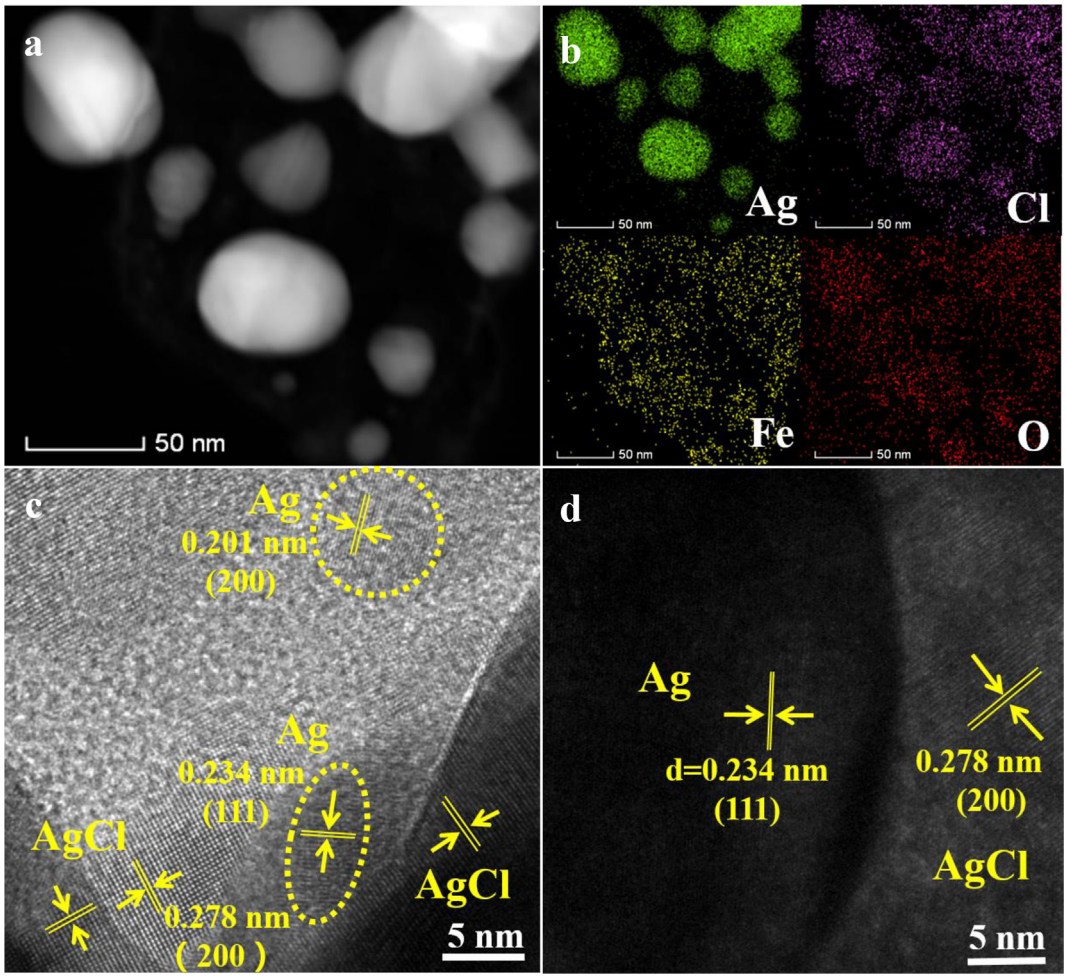

Fig. 3. (a) TEM images, (b) EDS mapping images of Ag, Cl, Fe, and O elements, (c) and (d) HRTEM images of 6%Ag/AgCl/Fh.

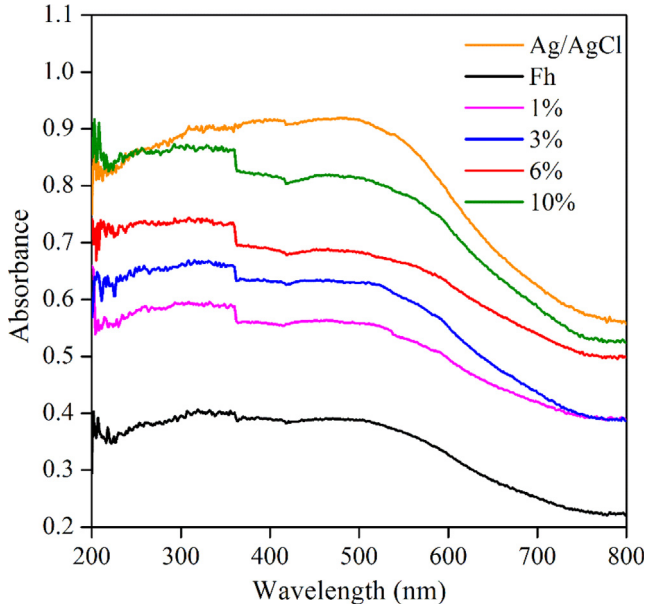

Fig. 4. UV–vis diffuse reflectance spectra of Ag/AgCl/Fh with various Ag contents.

reaction was also measured (Fig. 6d). Apparently, the Fe leaching concentrations of Ag/AgCl samples are lower than that of pure Fh in the whole process. Fe leaching increases with reaction time for all samples and then begins to decrease after 30 min, which can be also observed in Chen and Zhu [56]. They demonstrated that during the degradation of Orange II, some acidic intermediates could form in solution to induce the Fe^{3+} leaching from the catalysts. Similarly, some acidic intermediates could form in the degradation of BPA [57,58]. These acidic intermediates acid and Fe^{3+} may from complex, leading to Fe leaching from the catalyst. Afterwards, the Fe-complexed intermediates acid could be mineralized through the photo-Fenton reaction [59]. Finally, the dissolved Fe^{3+} could go back to the surface of catalysts. After 60 min, the concentration of Fe^{3+} is only 0.221 mg/L for 6%Ag/AgCl/Fh and 0.449 mg/L for pure Fh, indicating that Ag/AgCl can enhance the stability of Fh. Usually, the higher concentration of dissolved Fe can lead to higher catalysis efficiency for homogeneous Fenton catalysis. However, 6%Ag/AgCl/Fh exhibits higher degradation efficiency towards BPA as compared with pure Fh, which further proves the synergistic reaction between Ag/AgCl and Fh in the process of photo-Fenton catalysis.

The decomposition of H_2O_2 was also collected during the photo-Fenton catalysis (Fig. S6). H_2O_2 can hardly be decomposed in the absence of catalysts. The addition of Fh can evidently accelerate the decomposition of H_2O_2, and Ag/AgCl/Fh shows even better decomposition rate of H_2O_2. Nearly 98.1% H_2O_2 can be decomposed by the 6%Ag/AgCl/Fh. The enhancement of H_2O_2 decomposition rate may be ascribed to the high conversion rate of Fe^{3+} to Fe^{2+} due to the photogenerated electrons from Ag nanoparticles under the irradiation of visible light, which will be discussed in detail below.

To evaluate the long-term stability of 6%Ag/AgCl/Fh, the repeatability experiments of BPA degradation were further conducted

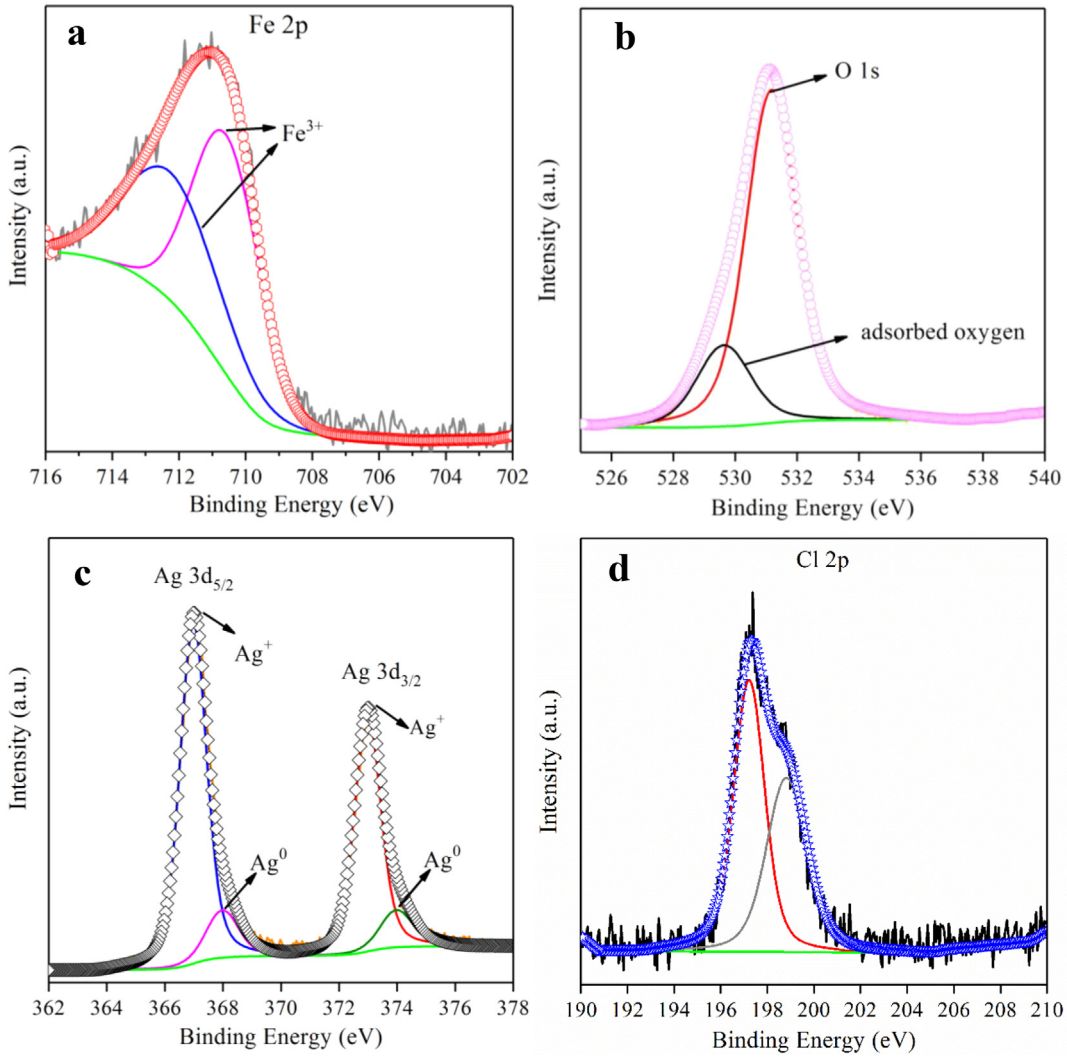

Fig. 5. XPS spectra of 6%Ag/AgCl/Fh sample: (a) Fe 2p, (b) O 1s; (c) Ag 3d, and (d) Cl 2p.

(Fig. 7a). The photo-Fenton catalytic activity of 6%Ag/AgCl/Fh on the degradation (100% for degradation rate) and mineralization (53.7% for TOC removal rate) of BPA remains quite efficient with a low Fe leaching of 0.334 mg/L after 4 recycles, indicating good stability of 6%Ag/AgCl/Fh. The slight decrease of the photo-Fenton catalytic performance may be attributed to the loss of the catalysts during the recovery process of the catalysts via centrifugation and the partial deactivation of the catalyst after several reuses [60]. The XRD patterns of 6%Ag/AgCl/Fh before and after 4 recycles were collected (Fig. 7b), which show no obvious changes, again indicating good structural stability of the composite.

3.3. Regeneration of Fe^{2+}

To verify the redox cycling of Fe^{2+}/Fe^{3+} in the photo-Fenton reaction, the concentration of Fe^{2+} on the surface of as-prepared samples during the degradation of BPA was measured (Fig. 8a). Few Fe^{2+} can be detected on the surface of catalyst for the pure Fh sample during the photo-Fenton reaction. After loading the Ag/AgCl on the surface of Fh, the concentration of Fe^{2+} increases evidently, indicating the introduced Ag/AgCl can accelerate the reduction from Fe^{3+} to Fe^{2+} by the photo-generated electrons under visible light. Moreover, the concentration of Fe^{2+} increases evidently in the first 30 min and then decreases for all samples, which may be attributed to the presence of H_2O_2 in the reaction system. The abundant H_2O_2 can oxidize the reduced Fe^{2+} to produce ·OH, resulting in the regeneration of Fe^{3+}. This curve trend of Fe^{2+} concentration can be also observed in other researches [23] [61]. Moreover, we also investigated the XPS spectra for Fe 2p on the surfaces of and 6%Ag/AgCl/Fh before and after the first and fourth degradation of BPA (Fig. 8b). No peaks for Fe^{2+} can be observed in the XPS spectra of fresh 6%Ag/AgCl/Fh catalyst. However, significant Fe^{2+} signals with the binding energy of 709.3 eV [50,62] appear both in XPS spectra of the catalysts after the first and forth degradation of BPA. In addition, the ratio of Fe^{2+} for the first reaction sample and the forth reaction sample are 0.25 and 0.27, respectively. It indicated the redox cycling of Fe^{3+}/Fe^{2+} could be achieved in the photo-Fenton reaction. The above results demonstrate that the reduction of Fe^{3+} to Fe^{2+} could be accelerated by the photo-generated electrons from Ag/AgCl under visible light.

3.4. Effect of initial pH

The influence of initial pH on the degradation of BPA was investigated at pH 3, 4, 5 and 6 (Fig. 9). The degradation efficiency of BPA is the highest at pH 3 and decreases with rising initial pH. When the initial pH varies from 3 to 6, the degradation rate of BPA decreases from 95.0% to 54.3% in 30 min, with the TOC removal rate decreasing from 89.3% to 43.7% in 60 min. The main reason for the decrease of photo-Fenton catalytic activity may be due to the decrease of ·OH oxidation potential with increasing pH. The oxidation potential of ·OH

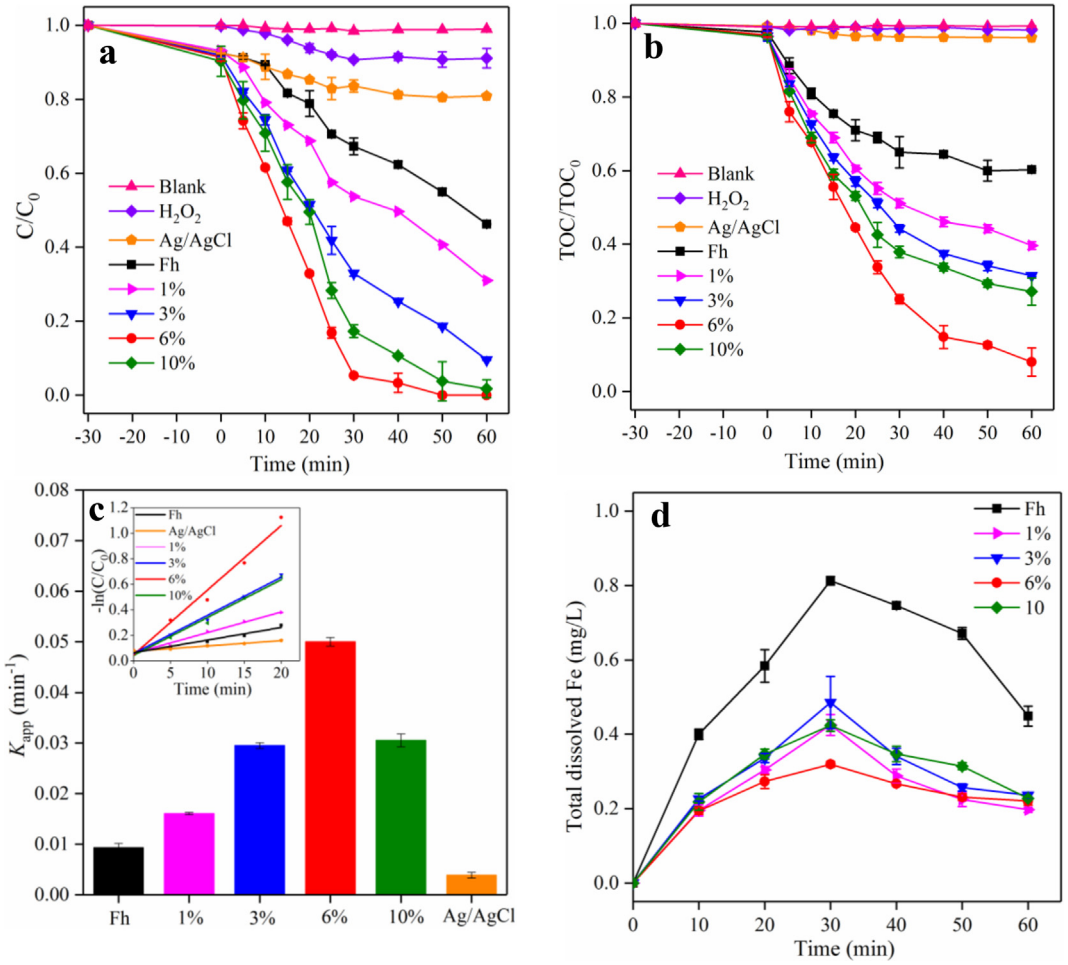

Fig. 6. (a) Degradation, (b) mineralization, and (c) apparent rate constants of BPA on different samples under visible light irradiation. Inset of (c): pseudo-first order kinetics for the photocatalytic degradation of BPA on these samples; (d) total dissolved iron concentration. [Catalyst dosage] = 1 g/L; [BPA] = 30 mg/L; [H_2O_2] = 10 mM; pH = 3.

ranges from 2.65 to 2.80 V at pH 3 and decreases to 1.90 V at pH 7 [23,63], which means that the oxidation ability of ·OH is stronger at near-acidic pH than at neutral pH. These observations are very consistent with those in previous studies [3,23,64]. On the other hand, the Fe leaching is relatively high at a low pH, which is beneficial for the Fenton reaction [27]. However, it should be stressed that at pH 6, which is very close to neutral pH, almost complete degradation could still be achieved within 60 min, although it takes longer reaction time than at pH 3. The results implies that the as-prepared samples still exhibit relatively high photo-Fenton catalytic activity at high pH value.

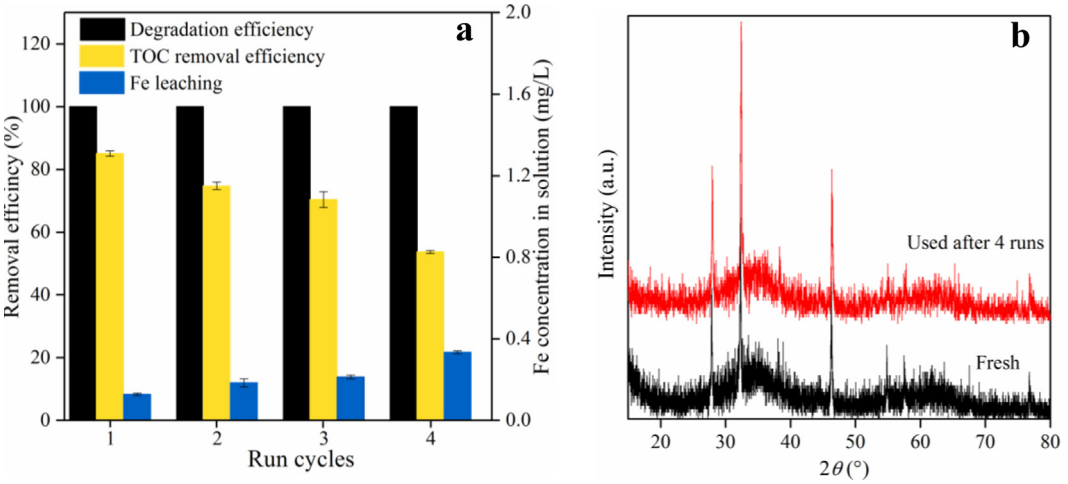

Fig. 7. (a) Stability test of 6%Ag/AgCl/Fh. [Catalyst dosage] = 1 g/L; [BPA] = 30 mg/L; [H_2O_2] = 10 mM; pH = 3; (b) XRD pattern of 6%Ag/AgCl/Fh before and after 4 recycles.

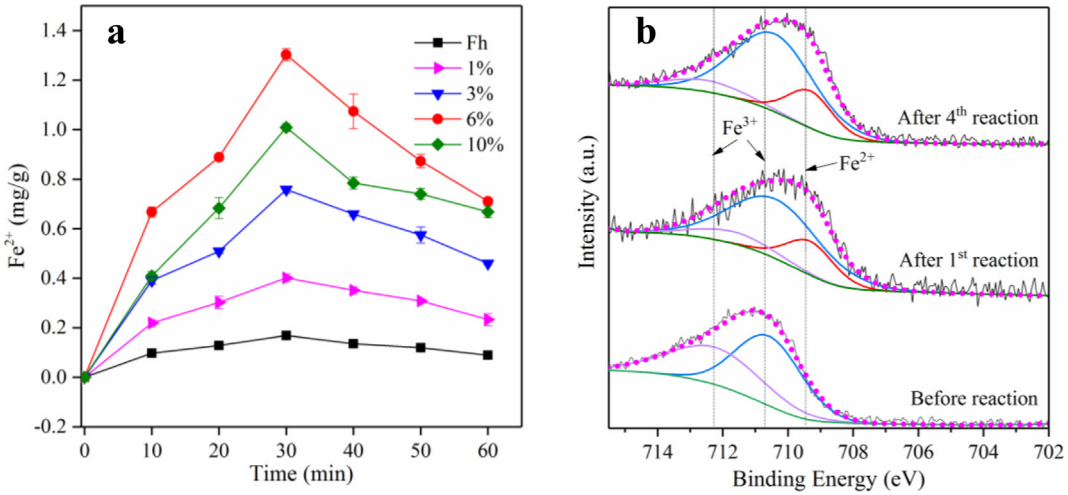

Fig. 8. (a) Concentration of Fe^{2+} on the surface of as-prepared samples during the photo-Fenton reaction. [Catalyst dosage] = 1 g/L; [BPA] = 30 mg/L; [H_2O_2] = 10 mM; pH = 3; (b) XPS spectra for Fe 2p on the surfaces of 6%Ag/AgCl/Fh before and after the first and fourth degradation of BPA.

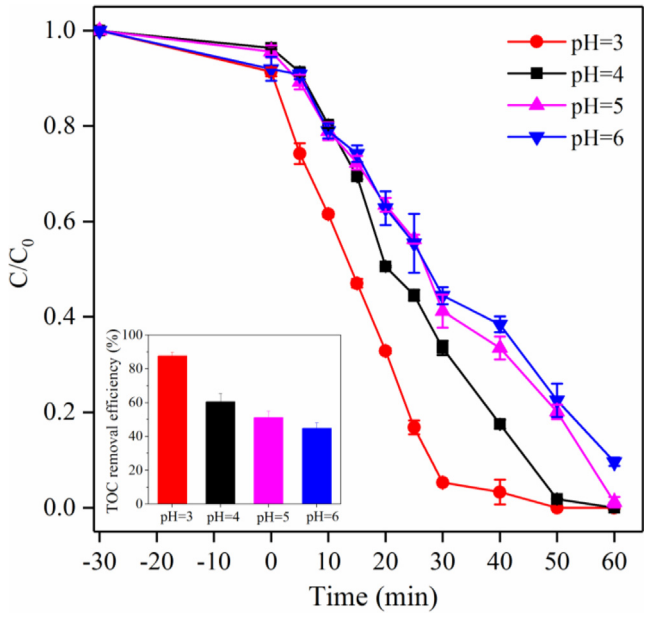

Fig. 9. Effect of pH on degradation and mineralization (Insert) of BPA on 6%Ag/AgCl/Fh under visible light irradiation. [Catalyst dosage] = 1 g/L; [BPA] = 30 mg/L; [H_2O_2] = 10 mM.

3.5. Effect of the initial H_2O_2 and catalyst dosage

The H_2O_2 dosage is an important parameter in the heterogeneous photo-Fenton reaction. The photo-Fenton catalytic efficiency increases with increasing the initial H_2O_2 from 4 to 10 mM (Fig. S7a), which results from the increase of ·OH generated from the decomposition of H_2O_2. With further increasing the initial H_2O_2 to 12 mM, the increase of the removal rate is negligible, which may be ascribed to that the redundant H_2O_2 may react with ·OH to hinder the photo-Fenton reaction. Also, the effect of 6%Ag/AgCl/Fh dosage on the degradation of BPA were also studied (Fig. S7b). When the dosage of 6%Ag/AgCl/Fh increases from 0.5 to 1.5 g/L, the degradation rate of BPA firstly increases and then decreases slightly as the catalyst dosage reaches 1.5 g/L. The results may be due to the high turbidity with the high catalyst dosage that would obstruct the penetration of light.

3.6. Effect of the irradiation time by a mercury lamp

To verify the impact of the ratio of reduced Ag nanoparticles, different 6%Ag/AgCl/Fh samples were synthesized at different irradiation time (0.5, 1, 2, and 3 h) using a mercury lamp and their photo-Fenton catalytic performances were tested by the degradation of BPA (Fig. 10). The XRD patterns of these samples were also collected (Fig. 10a). The reflection area of Ag (1 1 1) and AgCl (2 0 0) are selected to compare the change of the relative amount of Ag to AgCl at different irradiation time indirectly. Noticeably, the S_{Ag}/S_{AgCl} intensity ratio increases from 0.147 to 0.254 with increasing irradiation time, suggesting more Ag nanoparticles are reduced. The degradation rate of BPA increases slightly with the increase of irradiation time over 6%Ag/AgCl/Fh. The K_{app} value for the system of 3 h irradiation over 6%Ag/AgCl/Fh is 0.538 min^{-1}, which is only a little higher than that of 1 h irradiation over 6%Ag/AgCl/Fh (0.506 min^{-1}) (Fig. 10b). These results indicates that the increase of Ag nanoparticles could enhance the photo-Fenton catalytic activity of the composites due to the higher utilization of visible light; however, the increase of Ag nanoparticles through prolonging light irradiation is limited. Therefore, taking the production costs into account, the irradiation time for the reduction of Ag nanoparticles was chosen as 1 h in this work.

3.7. Analysis of active free radicals

The ESR with 5, 5-dimethyl-1-pyrroline N-oxide (DMPO) was further acquired to probe the reactive oxygen species produced on the surface of 6%Ag/AgCl/Fh under light irradiation (Fig. 11). No signals for DMPO – $\cdot O_2^-$ are observed in the methanol dispersion of 6%Ag/AgCl/Fh, no matter whether the reaction is conducted in darkness or under the irradiation of light. Four characteristic peaks with an intensity ratio of 1:2:2:1 are observed in the aqueous dispersion of 6%Ag/AgCl/Fh after the irradiation of a xenon lamp for 5 min, indicating that ·OH can be generated and plays an important role in the photo-Fenton reaction [28,65].

To provide direct evidence for the existence of ·OH. The concentrations of ·OH in the heterogeneous photo-Fenton reaction were measured using BA as an ·OH probe (Fig. 12). The concentrations of ·OH increases obviously after loading Ag/AgCl, suggesting that the combination of Ag/AgCl with Fh could accelerate the generation of ·OH. Noticeably, the ·OH concentration of 6%Ag/AgCl/Fh reaches 267.6 μmol/L, which is much higher than that of pure Fh (69.2 μmol/L).

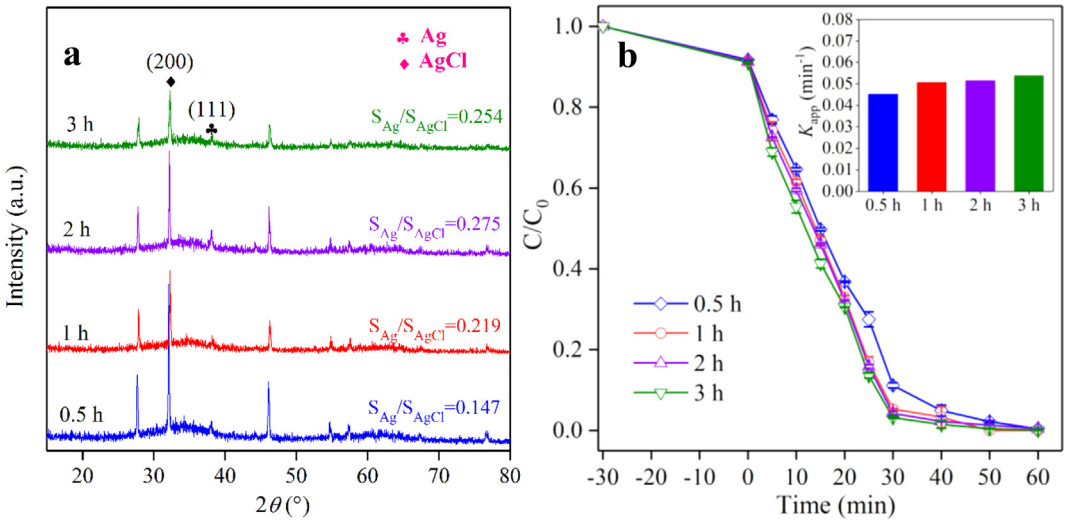

Fig. 10. (a) The XRD patterns of 6%Ag/AgCl/Fh under different UV irradiation time; (b) degradation and apparent rate constants (Insert) of BPA on different samples under visible light irradiation. [Catalyst dosage] = 1 g/L; [BPA] = 30 mM; [H_2O_2] = 10 mM.

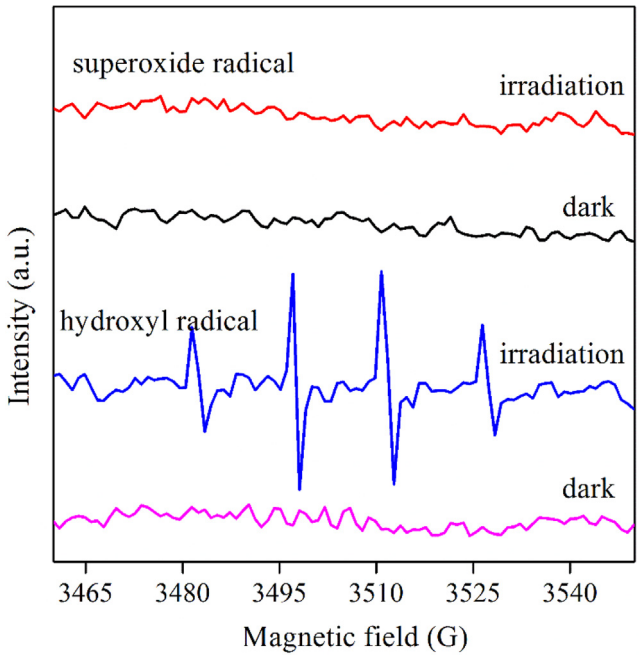

Fig. 11. DMPO spin-trapping ESR spectra recorded with 2%Ag/LDH in methanol dispersion (for DMPO−$\cdot O_2^-$) and aqueous dispersion (for DMPO−·OH) under irradiation of xenon lamp.

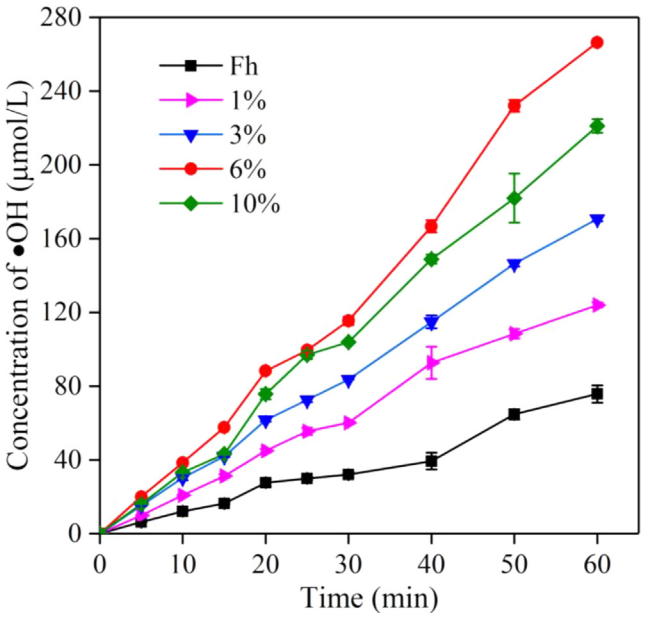

Fig. 12. The concentration of ·OH in the heterogeneous photo-Fenton reaction. [Catalyst dosage] = 1 g/L; [BA] = 10 mM; [H_2O_2] = 10 mM.

3.8. Photo-Fenton catalytic mechanism

As demonstrated above, Ag/AgCl/Fh photocatalysts have a high photo-Fenton catalytic activity for degradation of BPA, and the possible mechanisms for the enhancement in photo-Fenton catalytic activity of Ag/AgCl/Fh are schematically illustrated (Scheme 2). Under visible light irradiation, AgCl cannot be stimulated on account of the wide band gap of 3.25 eV [66]. However, according to many previous studies [34,67–69], Ag nanoparticles can absorb visible light and produce electron–hole pairs because of their SPR effect. The energy of the excited hot electrons can reach 1.0–4.0 eV for the Fermi level of noble metal [28,70]. Thus, the excited electrons have enough energy to transfer from Ag nanoparticles to the conduction band (CB) of AgCl, even though the CB of AgCl (0.08 eV) (Fig. S8) is lower than the Fermi energy of metallic Ag. As a result, the photogenerated electrons and holes are spatially isolated, which significantly inhibit their undesirable recombination. The photo generated electrons will further transfer from the CB of AgCl to the surface of Fh to participate in the conversion of

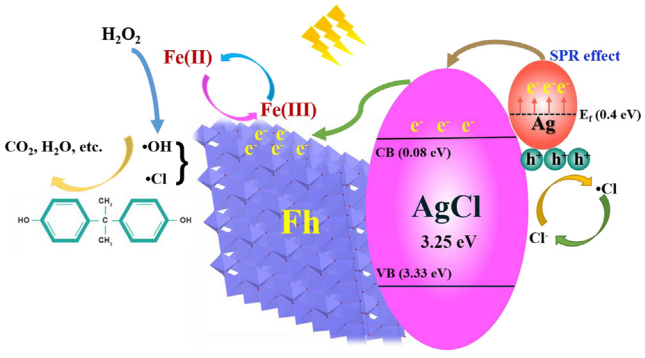

Scheme 2. Possible photocatalytic mechanism.

Fe^{3+} to Fe^{2+}. Subsequently, Fe^{2+} reacts with H_2O_2 to produce ·OH and can be oxidized to Fe^{3+} simultaneously. Therefore, the electrons from Ag nanoparticles can accelerate the redox cycling of Fe^{2+}/Fe^{3+} in heterogeneous Fenton reaction. The produced ·OH have remarkable efficiency for the degradation and mineralization of BPA. On the other hand, Many previous researches [33,43,71,72] pointed out that a certain amount of photogenerated holes originating from Ag may transfer to the surface of AgCl, thereby resulting in the oxidation of Cl^- to ·Cl. As ·Cl is a kind of reactive radical species, it should be able to oxidize the surface-adsorbed BPA and hence be reduced to Cl^- atoms again. The resultant ·Cl may react with Ag^+ to form AgCl, maintaining the stability of the as-prepared materials [67]. Possibly the production of ·Cl may also contribute to the enhanced degradation of BPA.

4. Conclusion

Plasmonic Ag/AgCl nanoparticles coated Fh with high photo-Fenton catalytic activity were successfully synthesized via a deposition–precipitation-photo reduction method. The photo-Fenton catalytic activities of Ag/AgCl/Fh composites for the degradation towards BPA are improved evidently compared with pure Fh. The concentration of dominant radicals (·OH) can even reach to 267.6 μmol/L after 60 min, which is much higher than that of pure Fh (69.2 μmol/L). The loading of Ag/AgCl can accelerate the redox cycling of Fe^{2+}/Fe^{3+} by the photo generated electrons from Ag nanoparticles due to the SPR effect under the visible light irradiation. On the other hand, Fh has a tailoring effect on Ag/AgCl to inhibit its aggregation. Therefore, more ·OH can be produced to attack the organic compounds. This study will motivate new developments in plasmonic photo-Fenton catalyst methodology and promote their practical application in environmental remediation.

Acknowledgments

This work was financially supported by the National Natural Science Foundation of China (41572031), National Program for Support of Top-notch Young Professionals, Guangdong Provincial Program for Support of Top-notch Young Professionals (2014TQ01Z249), and China Scholarship Council.

Appendix A. Supplementary data

Supplementary data associated with this article can be found, in the online version, at http://dx.doi.org/10.1016/j.cej.2018.04.073.

References

[1] D. Kassinos, N. Varnava, C. Michael, P. Piera, Homogeneous oxidation of aqueous solutions of atrazine and fenitrothion through dark and photo-Fenton reactions, Chemosphere 74 (2009) 866–872.
[2] G.M.S. ElShafei, F.Z. Yehia, O.I.H. Dimitry, A.M. Badawi, G. Eshaq, Degradation of nitrobenzene at near neutral pH using Fe^{2+}–glutamate complex as a homogeneous Fenton catalyst, Appl. Catal., B 99 (2010) 242–247.
[3] J.J. Pignatello, E. Oliveros, A. MacKay, Advanced oxidation processes for organic contaminant destruction based on the fenton reaction and related chemistry, Crit. Rev. Environ. Sci. Technol. 36 (2006) 1–84.
[4] O.A. Makhotkina, S.V. Preis, E.V. Parkhomchuk, Water delignification by advanced oxidation processes: Homogeneous and heterogeneous Fenton and H_2O_2 photo-assisted reactions, Appl. Catal., B 84 (2008) 821–826.
[5] J. Kiwi, C. Pulgarin, P. Peringer, Effect of Fenton and photo-Fenton reactions on the degradation and biodegradability of 2 and 4-nitrophenols in water treatment, Appl. Catal., B 3 (1994) 335–350.
[6] L.M. Nieto, G. Hodaifa, S. Rodríguez, J.A. Giménez, J. Ochando, Degradation of organic matter in olive-oil mill wastewater through homogeneous Fenton-like reaction, Chem. Eng. J. 173 (2011) 503–510.
[7] A. Georgi, M.V. Polo, K. Crincoli, K. Mackenzie, F.D. Kopinke, Accelerated catalytic Fenton reaction with traces of iron – An Fe-Pd-multicatalysis approach, Environ. Sci. Technol. 50 (2016) 5882.
[8] G. Subramanian, G. Madras, Remarkable enhancement of Fenton degradation at a wide pH range promoted by thioglycolic acid, Chem. Commun. 53 (2017) 1136–1139.
[9] Y. Hou, Y. Wang, H. Yuan, H. Chen, G. Chen, J. Shen, L. Li, The enhanced catalytic degradation of $SiO_2/Fe_3O_4/C@TiO_2$ photo-Fenton system on p-nitrophenol, J. Nanopart. Res. 18 (11) (2016) 343.
[10] X. Yang, W. Chen, J. Huang, Y. Zhou, Y. Zhu, C. Li, Rapid degradation of methylene blue in a novel heterogeneous Fe_3O_4 @rGO@TiO_2-catalyzed photo-Fenton system, Sci. Rep. 5 (2015) 10632.
[11] S. Wang, A comparative study of Fenton and Fenton-like reaction kinetics in decolourisation of wastewater, Dyes Pigments 76 (2008) 714–720.
[12] P. Malik, S. Saha, Oxidation of direct dyes with hydrogen peroxide using ferrous ion as catalyst, Sep. Purif. Technol. 31 (2003) 241–250.
[13] M.S. Lucas, J.A. Peres, Decolorization of the azo dye Reactive Black 5 by Fenton and photo-Fenton oxidation, Dyes Pigments 71 (2006) 236–244.
[14] M.E. Hassan, Y. Chen, G. Liu, D. Zhu, J. Cai, Heterogeneous photo-Fenton degradation of methyl orange by Fe_2O_3/TiO_2 nanoparticles under visible light, J. Water Process Eng. 12 (2016) 52–57.
[15] M.B. Kasiri, H. Aleboyeh, A. Aleboyeh, Degradation of Acid Blue 74 using Fe-ZSM5 zeolite as a heterogeneous photo-Fenton catalyst, Appl. Catal., B 84 (2008) 9–15.
[16] M. Dükkancı, G. Gündüz, S. Yılmaz, R. Prihod'ko, Heterogeneous Fenton-like degradation of Rhodamine 6G in water using CuFeZSM-5 zeolite catalyst prepared by hydrothermal synthesis, J. Hazard. Mater. 181 (2010) 343–350.
[17] N. Demir, G. Gündüz, M. Dükkancı, Degradation of a textile dye, Rhodamine 6G (Rh6G), by heterogeneous sonophotoFenton process in the presence of Fe-containing TiO_2 catalysts, Environ. Sci. Pollut. Res. 22 (2015) 3193–3201.
[18] L. Yu, J. Chen, Z. Liang, W. Xu, L. Chen, D. Ye, Degradation of phenol using Fe_3O_4-GO nanocomposite as a heterogeneous photo-Fenton catalyst, Sep. Purif. Technol. 171 (2016) 80–87.
[19] X. Wang, C. Liu, X. Li, F. Li, S. Zhou, Photodegradation of 2-mercaptobenzothiazole in the gamma-Fe_2O_3/oxalate suspension under UVA light irradiation, J Hazard Mater 153 (2008) 426–433.
[20] J. Xu, Y. Li, B. Yuan, C. Shen, M. Fu, H. Cui, W. Sun, Large scale preparation of Cu-doped α-FeOOH nanoflowers and their photo-Fenton-like catalytic degradation of diclofenac sodium, Chem. Eng. J. 291 (2016) 174–183.
[21] Z. Xu, M. Zhang, J. Wu, J. Liang, L. Zhou, B. L, Visible light-degradation of azo dye methyl orange using TiO_2/beta-FeOOH as a heterogeneous photo-Fenton-like catalyst, Water Sci. Technol. 68 (2013) 2178–2185.
[22] C. Cai, Z. Zhang, J. Liu, N. Shan, H. Zhang, D.D. Dionysiou, Visible light-assisted heterogeneous Fenton with $ZnFe_2O_4$ for the degradation of Orange II in water, Appl. Catal., B 182 (2016) 456–468.
[23] T. Xu, R. Zhu, G. Zhu, J. Zhu, X. Liang, Y. Zhu, H. He, Mechanisms for the enhanced photo-Fenton activity of ferrihydrite modified with $BiVO_4$ at neutral pH, Appl. Catal., B 212 (2017) 50–58.
[24] J.C. Barreiro, M.D. Capelato, L. Martin-Neto, H.C. Bruun Hansen, Oxidative decomposition of atrazine by a Fenton-like reaction in a H_2O_2/ferrihydrite system, Water Res. 41 (2007) 55–62.
[25] X. Zhang, Y. Chen, N. Zhao, H. Liu, Y. Wei, Citrate modified ferrihydrite microstructures: facile synthesis, strong adsorption and excellent Fenton-like catalytic properties, RSC Adv. 4 (2014) 21575–21583.
[26] D. Xu, Y. Zhang, F. Cheng, P. Dai, Efficient removal of dye from an aqueous phase using activated carbon supported ferrihydrite as heterogeneous Fenton-like catalyst under assistance of microwave irradiation, Taiwan Inst. Chem. Eng. 60 (2016) 376–382.
[27] H. Zeng, X. Liu, T. Wei, X. Li, T. Liu, X. Min, Q. Zhu, X. Zhao, J. Li, Boosting visible light photo-/Fenton-catalytic synergetic activity of $BiOIO_3$ by coupling with Fe_2O_3, RSC Adv. 7 (2017) 23787–23792.
[28] X. Li, S. Fang, L. Ge, C. Han, P. Qiu, W. Liu, Synthesis of flower-like Ag/AgCl-Bi_2MoO_6 plasmonic photocatalysts with enhanced visible-light photocatalytic performance, Appl. Catal., B 176–177 (2015) 62–69.
[29] B. Ma, J. Guo, W.-L. Dai, K. Fan, Ag-AgCl/WO_3 hollow sphere with flower-like structure and superior visible photocatalytic activity, Appl. Catal., B 123–124 (2012) 193–199.
[30] D. Xu, W. Shi, C. Song, M. Chen, S. Yang, W. Fan, B. Chen, In-situ synthesis and enhanced photocatalytic activity of visible-light-driven plasmonic Ag/AgCl/$NaTaO_3$ nanocubes photocatalysts, Appl. Catal., B 191 (2016) 228–234.
[31] H. Li, Y. Sun, B. Cai, S. Gan, D. Han, L. Niu, T. Wu, Hierarchically Z-scheme photocatalyst of Ag@AgCl decorated on $BiVO_4$ (040) with enhancing photoelectrochemical and photocatalytic performance, Appl. Catal., B 170–171 (2015) 206–214.
[32] J. Hou, C. Yang, Z. Wang, Q. Ji, Y. Li, G. Huang, S. Jiao, H. Zhu, Three-dimensional Z-scheme AgCl/Ag/γ-TaON heterostructural hollow spheres for enhanced visible-light photocatalytic performance, Appl. Catal., B 142–143 (2013) 579–589.
[33] G. Begum, J. Manna, R.K. Rana, Controlled orientation in a bio-inspired assembly of Ag/AgCl/ZnO nanostructures enables enhancement in visible-light-induced photocatalytic performance, Chemistry 18 (2012) 6847–6853.
[34] H. Zhang, X. Fan, X. Quan, S. Chen, H. Yu, Graphene sheets grafted Ag@AgCl hybrid with enhanced plasmonic photocatalytic activity under visible light, Environ. Sci. Technol. 45 (2011) 5731–5736.
[35] X. Yan, X. Wang, W. Gu, M. Wu, Y. Yan, B. Hu, G. Che, D. Han, J. Yang, W. Fan, W. Shi, Single-crystalline $AgIn(MoO_4)_2$ nanosheets grafted Ag/AgBr composites with enhanced plasmonic photocatalytic activity for degradation of tetracycline under visible light, Appl. Catal., B 164 (2015) 297–304.
[36] F. Chen, H. Huang, C. Zeng, X. Du, Y. Zhang, Achieving enhanced UV and visible light photocatalytic activity for ternary Ag/AgBr/$BiOIO_3$: decomposition for diverse industrial contaminants with distinct mechanisms and complete mineralization ability, ACS Sustain. Chem. Eng. 5 (9) (2017) 7777–7791.
[37] M. Zhu, P. Chen, M. Liu, Graphene oxide enwrapped Ag/AgX (X = Br, Cl) nanocomposite as a highly efficient visible-light plasmonic photocatalyst, ACS Nano 5

(6) (2011) 4529.
[38] L. Ye, J. Liu, C. Gong, L. Tian, T. Peng, L. Zan, Two Different roles of metallic Ag on Ag/AgX/BiOX (X = Cl, Br) visible light photocatalysts: surface plasmon resonance and Z-scheme bridge, ACS Catal. 2 (8) (2012) 1677–1683.
[39] H. Daupor, S. Wongnawa, Flower-like Ag/AgCl microcrystals: synthesis and photocatalytic activity, Mater. Chem. Phys. 159 (2015) 71–82.
[40] F. Chen, Q. Yang, C. Niu, X. Li, C. Zhang, G. Zeng, Plasmonic photocatalyst Ag@AgCl/ZnSn(OH)$_6$: synthesis, characterization and enhanced visible-light photocatalytic activity in the decomposition of dyes and phenol, RSC Adv. 5 (2015) 63152–63164.
[41] D. Wang, Y. Li, G. Li Puma, C. Wang, P. Wang, W. Zhang, Q. Wang, Ag/AgCl@helical chiral TiO_2 nanofibers as a visible-light driven plasmon photocatalyst, Chem. Commun. 49 (2013) 10367–10369.
[42] J. Liu, R. Zhu, T. Xu, Y. Xu, F. Ge, Y. Xi, J. Zhu, H. He, Co-adsorption of phosphate and zinc (II) on the surface of ferrihydrite, Chemosphere 144 (2015) 1148–1155.
[43] J. Gamage McEvoy, W. Cui, Z. Zhang, Synthesis and characterization of Ag/AgCl–activated carbon composites for enhanced visible light photocatalysis, Appl. Catal., B 144 (2014) 702–712.
[44] R.M. Sellers, Spectrophotometric determination of hydrogen peroxide using potassium titanium(IV) oxalate, Analyst 105 (1980) 950–954.
[45] S.H. Joo, A.J. Feitz, D.L. Sedlak, T.D. Waite, Quantification of the oxidizing capacity of nanoparticulate zero-valent iron, Environ. Sci. Technol. 39 (2005) 1263–1268.
[46] P. Zhang, S. Yuan, P. Liao, Mechanisms of hydroxyl radical production from abiotic oxidation of pyrite under acidic conditions, Geochim. Cosmochim. Acta 172 (2016) 444–457.
[47] C.R. Keenan, D.L. Sedlak, Factors affecting the yield of oxidants from the reaction of nanoparticulate zero-valent iron and oxygen, Environ. Sci. Technol. 42 (2008) 1262–1267.
[48] M.K. Seery, R. George, P. Floris, S.C. Pillai, Silver doped titanium dioxide nanomaterials for enhanced visible light photocatalysis, J. Photochem. Photobiol., A 189 (2007) 258–263.
[49] Y. Zhu, R. Zhu, G. Zhu, M. Wang, Y. Chen, J. Zhu, Y. Xi, H. He, Y. Zhu, R. Zhu, Plasmonic Ag coated Zn/Ti-LDH with excellent photocatalytic activity, Appl. Surf. Sci. 433 (2018) 458–467.
[50] Y. Lee, W. Lee, Degradation of trichloroethylene by Fe(II) chelated with cross-linked chitosan in a modified Fenton reaction, J. Hazard. Mater. 178 (2010) 187–193.
[51] V. Khare, M. Mullet, K. Hanna, M. Blumers, M. Abdelmoula, G. Klingelhöfer, C. Ruby, Comparative studies of ferric green rust and ferrihydrite coated sand: role of synthesis routes, Solid State Sci. 10 (2008) 1342–1351.
[52] P. Wang, B. Huang, Z. Lou, X. Zhang, X. Qin, Y. Dai, Z. Zheng, X. Wang, Synthesis of highly efficient Ag@AgCl plasmonic photocatalysts with various structures, Chemistry 16 (2010) 538–544.
[53] X. Yao, X. Liu, One-pot synthesis of Ag/AgCl@SiO_2 core–shell plasmonic photocatalyst in natural geothermal water for efficient photocatalysis under visible light, J. Mol. Catal. A: Chem. 393 (2014) 30–38.
[54] X. Yao, X. Liu, D. Zhu, C. Zhao, L. Lu, Synthesis of cube-like Ag/AgCl plasmonic photocatalyst with enhanced visible light photocatalytic activity, Catal. Commun. 59 (2015) 151–155.
[55] S. Guo, G. Zhang, J.C. Yu, Enhanced photo-Fenton degradation of rhodamine B using graphene oxide-amorphous $FePO_4$ as effective and stable heterogeneous catalyst, J. Colloid Interface Sci. 448 (2015) 460–466.
[56] J. Chen, L. Zhu, Comparative study of catalytic activity of different Fe-pillared bentonites in the presence of UV light and H_2O_2, Sep. Purif. Technol. 67 (2009) 282–288.
[57] N. Lu, Y. Lu, F. Liu, K. Zhao, X. Yuan, Y. Zhao, Y. Li, H. Qin, J. Zhu, $H_3PW_{12}O_{40}$/TiO_2 catalyst-induced photodegradation of bisphenol A (BPA): kinetics, toxicity and degradation pathways, Chemosphere 91 (2013) 1266.
[58] J. Sharma, I.M. Mishra, D.D. Dionysiou, V. Kumar, Oxidative removal of Bisphenol A by UV-C/peroxymonosulfate (PMS): kinetics, influence of co-existing chemicals and degradation pathway, Chem. Eng. J. 276 (2015) 193–204.
[59] A. Bozzi, T. Yuranova, J. Mielczarski, J. Kiwi, Evidence for immobilized photo-Fenton degradation of organic compounds on structured silica surfaces involving Fe recycling, New J. Chem. 28 (2004) 519.
[60] M. Yadav, V. Singh, Y.C. Sharma, Methyl transesterification of waste cooking oil using a laboratory synthesized reusable heterogeneous base catalyst: Process optimization and homogeneity study of catalyst, Energy Convers. Manage. 148 (2017) 1438–1452.
[61] Z. Ma, L. Ren, S. Xing, Y. Wu, Y. Gao, Sodium Dodecyl sulfate modified $FeCo_2O_4$ with enhanced Fenton-like activity at neutral pH, J. Phys. Chem. C 119 (2015) 23068–23074.
[62] X. Hu, B. Liu, Y. Deng, H. Chen, S. Luo, C. Sun, P. Yang, S. Yang, Adsorption and heterogeneous Fenton degradation of 17α-methyltestosterone on nano Fe_3O_4/MWCNTs in aqueous solution, Appl. Catal., B 107 (2011) 274–283.
[63] A. Babuponnusami, K. Muthukumar, Advanced oxidation of phenol: a comparison between Fenton, electro-Fenton, sono-electro-Fenton and photo-electro-Fenton processes, Chem. Eng. J. 183 (2012) 1–9.
[64] J. Feng, X. Hu, P.L. Yue, H.Y. Zhu, G.Q. Lu, Discoloration and mineralization of Reactive Red HE-3B by heterogeneous photo-Fenton reaction, Water Res. 37 (2003) 3776–3784.
[65] H. Liu, Z. Chen, Y. Wang, Plasmonic Ag coated $BiOBr_{0.2}I_{0.8}$ nanosheets grown on graphene with excellent visible-light photocatalytic activity, J. Photochem. Photobiol. A 326 (2016) 30–40.
[66] J. Tejeda, N.J. Shevchik, W. Braun, A. Goldmann, M. Cardona, Valence bands of AgCl and AgBr: uv photoemission and theory, Phys. Rev. B 12 (1975) 1557–1566.
[67] S. Lin, L. Liu, Y. Liang, W. Cui, Z. Zhang, Oil-in-water self-assembled synthesis of Ag@AgCl nano-particles on flower-like $Bi_2O_2CO_3$ with enhanced visible-light-driven photocatalytic activity, Materials 9 (2016) 486.
[68] L. Ai, C. Zhang, J. Jiang, Hierarchical porous AgCl@Ag hollow architectures: self-templating synthesis and highly enhanced visible light photocatalytic activity, Appl. Catal., B 142–143 (2013) 744–751.
[69] C. An, S. Peng, Y. Sun, Facile synthesis of sunlight-driven AgCl: Ag plasmonic nanophotocatalyst, Adv. Mater. 22 (2010) 2570–2574.
[70] S. Linic, P. Christopher, D.B. Ingram, Plasmonic-metal nanostructures for efficient conversion of solar to chemical energy, Nat. Mater. 10 (2011) 911–921.
[71] S. Kang, Y. Fang, Y. Huang, L.-F. Cui, Y. Wang, H. Qin, Y. Zhang, X. Li, Y. Wang, Critical influence of g-C_3N_4 self-assembly coating on the photocatalytic activity and stability of Ag/AgCl microspheres under visible light, Appl. Catal., B 168–169 (2015) 472–482.
[72] J. Ke, C. Niu, J. Zhang, G. Zeng, Significantly enhanced visible light photocatalytic activity and surface plasmon resonance mechanism of Ag/AgCl/$ZnWO_4$ composite, J. Mol. Catal. A: Chem. 395 (2014) 276–282.